Environmental
Science
Water Research & Technology

ROYAL SOCIETY
OF CHEMISTRY

PAPER

View Article Online
View Journal | View Issue

Check for updates

Cite this: *Environ. Sci.: Water Res. Technol.*, 2021, **7**, 1748

Elementary reaction-based kinetic model for the fate of *N*-nitrosodimethylamine under UV oxidation†

Benjamin Barrios, Divya Kamath, Erica Coscarelli and Daisuke Minakata *

Received 15th April 2021,
Accepted 6th August 2021

DOI: 10.1039/d1ew00262g

rsc.li/es-water

UV photolysis is an effective process to remove nitrosamines from contaminated water resources. Nitrosamines represent a class of compounds with high potential for carcinogenicity and, therefore, there are serious concerns regarding their threat to human health and their environmental toxicity. Although the photochemical parameters of parent nitrosamines and their initial reaction pathways are well understood, the fate of nitrogen-containing species and reactive nitrogen species generated from nitrosamine degradation has not yet been elucidated. In this study, we develop an elementary reaction-based kinetic model for the photolysis of *N*-nitrosodimethylamine (NDMA) and the photochemical transformation products. We use density functional theory quantum mechanical calculations to calculate the aqueous-phase free energies of activation and reaction to investigate the kinetics and thermodynamics properties of the elementary reactions. We generate ordinary differential equations for all species involved in the identified reactions and solve them to obtain the time-dependent concentration profiles of NDMA and the degradation products at pH 3 and pH 7. The profiles are compared to experimental results in the literature to validate our elementary reaction-based kinetic model. This is the first study to develop an elementary reaction-based kinetic model for the photochemical reaction of NDMA and reactive nitrogen species. The findings of this study have a significant impact on the active research area of nitrosative stress and advanced oxidation processes that utilize nitrogen-containing compounds such as UV/nitrate and UV/chloramine advanced oxidation processes.

Water impact

UV photolysis is employed in water treatment and reuse practices. Understandings of photolysis-induced radical-involved basic reaction mechanisms enables the predictions of contaminants' fate not only in engineered but also natural aquatic environmental systems.

Introduction

A group of nitrosamines present in water imposes high potential for carcinogenicity and is of serious concern about their threat to human health in potable waters and adverse ecotoxicological effects in environmental waters.[1] Although the potential formation of some disinfection byproducts (DBPs) such as iodinated trihalomethanes may occur, with an increase in the use of chloramine as a primary/secondary disinfectant to reduce the formation of trihalomethanes, haloacetic acids, and other halogenated disinfection DBPs, more *N*-nitrosamines than in the past have been detected in drinking water,[2] wastewater, and wastewater reclamation processes.[3] The U.S. EPA calculated a screening level of 0.11 ng L^{-1} for *N*-nitrosodimethylamine (NDMA), one of the most commonly detected and carcinogenic *N*-nitrosamines, for tap water based on a 10^{-6} lifetime excess cancer risk.[4] In California, a 1.2-log NDMA removal is required for potable reuse of wastewater and the water reuse utilities must implement treatment processes that achieve the NDMA notification level of maximum of 10 ng L^{-1} in the reclaimed water.[5]

N-Nitrosamines preferably undergo photolysis, which results in the degradation of the parent structure containing N–NO bond. While the parameters of the photochemical reactions of parent nitrosamine compounds are well understood[6] such as the quantum yield, pH effect,[7,8]

Department of Civil and Environmental Engineering, Michigan Technological University, 1400 Townsend Drive, Houghton, MI, 49931, USA.
E-mail: dminakat@mtu.edu; Fax: +1 906 487 2943; Tel: +1 906 487 1830

† Electronic supplementary information (ESI) available: Additional information for the aqueous-phase computational calculations, molecular oxidation addition, Marcus theory, experimental apparatus and procedures, sensitivity analysis, toxicity calculations, TD-DFT analysis, thermodynamic properties in the presence of explicit water molecules, absorbance of HCHO, and experimentally proposed NDMA and reactive nitrogen species photochemical degradation pathways, linear free energy relationships and *xyz*-matrix of all transition states is given in the electronic ESI. See DOI: 10.1039/d1ew00262g

dissolved oxygen effect,[9] and initial reaction pathways,[7] the fate of nitrogen-containing species and reactive nitrogen species generated from the degradation of nitrosamine has not yet been elucidated. For example, each quantum yield of nitrogen species under the degradation of *N*-nitrosamines is not known. The reaction pathways and kinetics of peroxynitrite/peroxynitrous acid ($ONOO^-/ONOOH$)[10] with other degradation products of *N*-nitrosamines are not understood. Neither the kinetics of the reactions involving reactive nitrogen species nor the photochemical fate of nitrate/nitrite/peroxynitrite are fully understood.[11–14] Short-lived reactive nitrogen species are difficult to identify experimentally due to the lack of probe compounds and therefore it is not clear whether the experimentally reported rate constants represent the overall or elementary reaction steps. Consequently, challenges remain in identifying the elementary reaction pathways that are embedded in the overall photochemical degradation of *N*-nitrosamines. For these reasons, no mechanistic kinetic model of nitrosamines undergoing UV photolysis has been developed. Understanding the elementary reaction pathways and their kinetics enables the comprehensive prediction of the photochemical fate of nitrogen-containing compounds.

Density functional theory (DFT) quantum mechanical (QM) calculations provide complementary information about the kinetics and thermodynamics of elementary reactions to experimentally identified overall or elementary reaction steps.[16–22] QM calculations have been successfully used for the pathways of NDMA formation induced by ozonation.[15] Thorough analysis of both thermodynamics and kinetics of each elementary reaction is important as experimentally determined rate constants do not always provide the reaction mechanisms. The thermodynamics (*i.e.*, endergonic or exergonic) of elementary reactions can be determined by calculating the aqueous-phase free energies of reaction and the kinetics can be determined by calculating the aqueous-phase free energies of activation.[23,24] However, kinetics override thermodynamics for many radical reactions[25] and thus even though an elementary reaction is endergonic, the reaction may occur kinetically or there might be a backward reaction that may overtake a forward reaction. A kinetic model developed without the critical analysis of each elementary reaction or by blindly accepting literature-reported rate constants may fail to predict the fate of a target compound. For the aqueous-phase fate of nitrosamine where nitrogen-centered radicals are involved, challenges remain to identify the transition states or precursor complexes because of their possible shallow potential energy surfaces of singlet biradical reactions and the loose intermolecular bonds.[26–28]

In this study, we investigate the photolysis of NDMA and the photochemical products with DFT QM calculations to identify the elementary reaction pathways. Although the rate constants of major reactions involving the fate of NDMA degradation are experimentally determined and reported, it is important to evaluate each elementary reaction based on our calculated thermodynamics and kinetic properties because each rate constant is generally obtained by independent studies under the different experimental conditions. Once we understand the elementary reaction mechanism of all possible reactions that are involved in the NDMA degradation, we generate ordinary differential equations (ODEs) for all species involved in the identified reactions and solve them to obtain the time-dependent concentration profiles of NDMA and the degradation products at different pH values. The numerical solution of ODEs is critical to understand the fate that is determined by both species concentrations and reaction rate constants of all the elementary reactions. The profiles are compared to those obtained experimentally in the literature to validate our elementary reaction-based kinetic model.

Materials and methods

All of the QM calculations were performed using the Michigan Tech high-performance cluster "Superior" and homemade LINUX workstations. All the DFT calculations were conducted with the Gaussian 16 revision A. 01. program.[29] Single point energy calculations using the unrestricted coupled-cluster theory[30] with single, double, and noniterative triplet excitations (UCCSD(T)) were conducted with the Molpro package.[31] The unrestricted form of UM06-2X[32]/Aug-cc-pVTZ level of theory was used to calculate the wavefunction for a given molecular and radical structures and calculate the frequencies in both the gas and aqueous phases because of the previous applications.[33,34] The augmented basis set was recommended to optimize the ionized molecular and radical structure by including the diffuse function.[35] To avoid false convergence due to small gradients on a flat potential energy surface, we used the 'ultrafine' integration grid in the self consistent field procedure and geometry optimization. The aqueous-phase structures and frequencies were obtained using an implicit polarizable continuum model [universal solvation model (SMD)].[36] To verify the impact by the multireference state (*e.g.*, ground state oxygen molecule and the addition reaction and see the detailed analysis for Text S2 in the ESI†), we used hybrid single reference DFT, M05/Aug-cc-pVTZ,[35] as this method was previously used for the NDMA system in the literature.[15] It was shown that unrestricted DFT (UDFT) performed well in comparison to multireference methods for deriving energies and geometries of singlet biradical.[37,38] For the radical–radical coupling reactions, we used a NoSymmetry keyword to prevent the reorientation of molecules and radicals and guess = mix for broken-symmetry approach. Spin contamination resulting from the use of UDFT was corrected for some transition states and the detailed method is given in Text S1 in the ESI.† We also performed the stability test for the optimized transition states routinely using a keyword 'Stable'. To ensure the correct assignment to a local minima and a transition state, we analyzed the harmonic vibrational frequency. All transition states were verified by intrinsic reaction coordinate

(IRC)[39,40] to ensure the connection among reactants, transition states and products in particular for the radical–radical coupling reactions. We paid special attention to the spin contamination in the systems studied. The detailed calculation procedures are found in Text S1 of the ESI.† Marcus theory[41,42] was used to calculate the activation energy for single electron transfer and the detailed procedure is provided in Text S3 and Fig. S1 in the ESI.† It is noted that we did not intend to obtain the absolute energy values of each reaction as this is computationally demanding and prohibitive in getting accuracy values in the aqueous phase; however, we aimed to obtain the relative energies accurate enough to evaluate the relative energies resulting from various structures under the same reaction mechanism.

Once the elementary reaction pathways and the corresponding reaction rate constants were identified, we numerically solved the ODEs using the Gear method[43] by modifying the original UV/H_2O_2 kinetic model[44] and compared them to the experimental results reported in the literature. Experimental studies were performed and reported by Lee *et al.* (2005).[7] Text S4 in the ESI† summarizes the detailed experimental conditions. To evaluate the impact of each reaction rate constant on the simulated time-dependent concentration profiles, classical local sensitivity analysis was conducted. Text S5 in the ESI† provides the procedure, the results and a discussion of the sensitivity analysis.

Results and discussion

Overall results

Fig. 1 displays the time-dependent concentration profiles of NDMA, the major transformation products [*i.e.*, methylamine

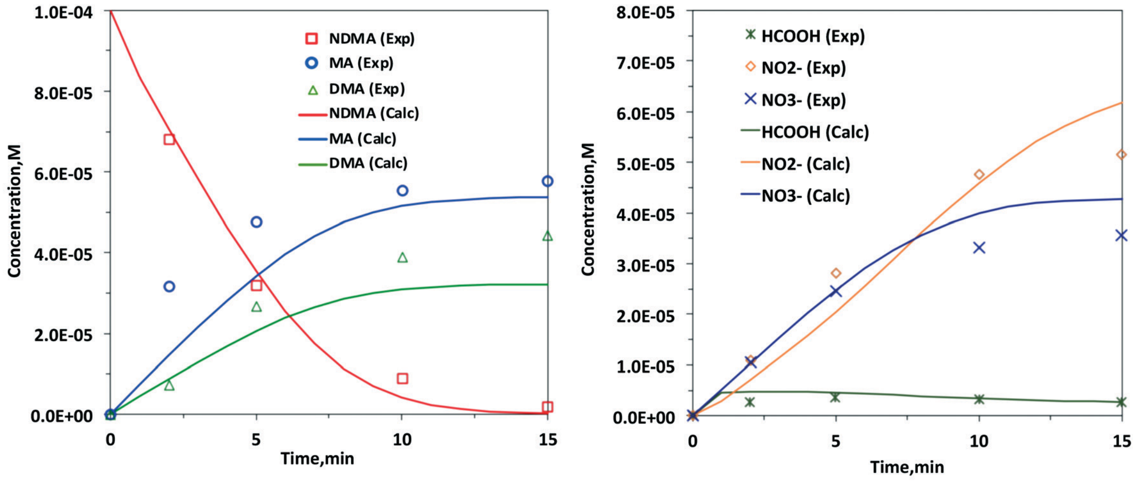

pH 7

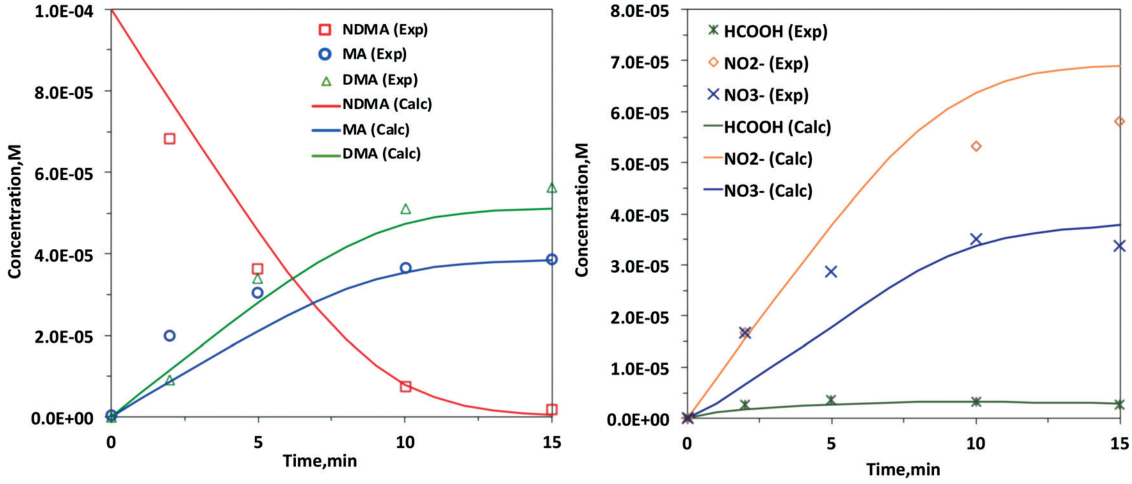

pH 3

Fig. 1 Experimental (exp)[7] and predicted (calc) time-dependent concentration profiles of NDMA and the transformation products at pH 7 (above) and pH 3 (below).

(MA) and dimethylamine (DMA)] and the minor transformation products [*i.e.*, formic acid (HCOOH), nitrite (NO_2^-), and nitrate (NO_3^-)] predicted at two pH values (pH 7 and pH 3) by our elementary reaction-based kinetic model and experimental studies in the literature.[7] We chose pH 3 because the photochemical fate at pH 3 represents those in the acid solution (*i.e.*, typical practices in direct potable reuse) as compared to those in the neutral solution. Table 1 includes the photochemical elementary reaction pathways identified in this study, the theoretically calculated free energies of activation, $\Delta G^{act}_{aq,calc}$, kcal mol^{-1}, the free energies of reaction, $\Delta G^{act}_{aq,calc}$, kcal mol^{-1}, activation energies, $\Delta E^{act}_{aq,calc}$, kcal mol^{-1}, imaginary frequency of the transition states, the k values in the literature, and the known pK_a values of each species that undergoes dissociation. It is important to track the dissociation/nondissociation of species at different pH values because of the various pK_a values of different species and the different reactivities between dissociated and nondissociated species. The sample deviation (SD) was calculated as shown in eqn (1) to evaluate the discrepancy between the predicted profiles by our elementary reaction-based kinetic model and the experimental values in the literature.

$$\mathrm{SD}_i = \sqrt{\left(\frac{1}{N_i - 1}\right)\sum_{j=1}^{N_i}\left[\frac{(C_{\exp,j} - C_{\mathrm{calc},j})}{C_{\exp,j}}\right]^2} \qquad (1)$$

where N_i is the total number of data points for species i, and $C_{\exp,j}$ and $C_{\mathrm{calc},j}$ are the experimental and calculated concentrations of species, i, respectively, for the j set of all times for which each data point is available. The SD value was calculated by weighting all data equally by dividing the difference between the experimental and calculated values by the experimental data, so that the outweighed data point(s) did not significantly affect the overall SD value for each species. The SD values were calculated as 0.27 for NDMA, 0.18 for DMA, 0.31 for MA, 0.23 for NO_2^-, 0.10 for NO_3^-, and 0.48 for HCOOH at pH 7. At pH 3, the SD value was 0.15 for NDMA, 0.16 for DMA, 0.33 for MA, 0.12 for NO_2^-, 0.36 for NO_3^-, and 0.23 for HCOOH. The SD values represent the statistical accuracy of predicted values as compared to the experimental observations. Although no kinetic model was previously developed and no comparison with other studies was possible, these SD values are reasonable from the results of our previously developed elementary reaction-based kinetic model for UV/H_2O_2 and UV/free chlorine AOPs.[23,24] It should be noted that the time-dependent concentration profiles of formaldehyde (HCHO) at both pH values were not included in Fig. 1 because HCHO is rapidly hydrolyzed to produce methylene glycol, $CH(OH)_2$. The $CH(OH)_2$ then partially undergoes a slow dimerization to dimethylene glycol, HO–CH_2OCH_2OH.[45] The pK_a value HCHO hydration was −3.36 and the hydration rate constants were reported as 10 M^{-1} s^{-1} at neutral pH and 5.37×10^3 M^{-1} s^{-1} at acid pH.[46,47] This approach to HCHO and $CH(OH)_2$ chemistry was successfully validated in our previous study[23] and these rate constants were used in this work. The $CH(OH)_2$ further reacts with ONOOH/$ONOO^-$ (see the details below).

Photolysis pathways and quantum yields of NDMA

We performed TD-DFT calculations at the level of M06-2X/Aug-cc-pVTZ with the SMD solvation model to reveal highest occupied molecular orbital (HOMO) and lowest unoccupied molecular orbital (LUMO) for the corresponding transition. We confirmed the $n \rightarrow \pi^*$ transition at 347 nm and the $\pi \rightarrow \pi^*$ transition at 202 nm, whose absorbance peaks are consistent with experimental observations at 332 nm and 228 nm.[3,8] The detailed TD-DFT method and results about MO are given in Text S6 and Fig. S3 in the ESI.†

The photolysis of NDMA by the 253.7 nm radiation emitted from a low-pressure UV lamp results in products *via* three major pathways: (1) homolytic cleavage of the N–NO bond of NDMA to produce aminium radicals [$(CH_3)_2$-$N^{\bullet}H^+$] and nitric oxide ($NO^{\bullet}$) (pathway 1 in Table 1); (2) heterolytic cleavage of the N–NO bond to produce dimethylamine [$(CH_3)_2NH_2^+$] and nitrous acid (HNO_2) (pathway 2); and (3) photooxidation in the presence of dissolved oxygen to produce *N*-methylidenmethylamine ($CH_2{=}N^+HCH_3$), $NO^{\bullet}$, and superoxide anion ($O_2^{\bullet-}$) radicals (pathway 3). For the elementary reaction-based kinetic model, we included the photolysis of NDMA degradation products such as nitrate (pathways 4 and 5),[48] nitrite (pathway 6), and peroxynitrite ion (pathway 7),[49] although these pathways may not be the major ones for the productions of $ONOO^-$, $NO^{\bullet}$, $HO^{\bullet}$ and $O_2^{\bullet-}$. These photolysis reactions are well known and are reported in the literature, and we use these reactions for our kinetic model (Table 1). We determined the partial quantum yields of each photochemical reaction at pH 7 and 3 by fitting with the time-dependent concentration profiles of each species obtained by the experiments (see the detailed procedure in the following sections). The overall quantum yield for NDMA degradation is well known to be 0.31 at pH 2–8.[9] We determined a quantum yield of 0.02 for pathway 1, 0.20 for pathway 2, and 0.12 for pathway 3 at pH 7. At pH 3, a partial quantum yield of 0.05 for pathway 1, 0.18 for pathway 2, and 0.27 for pathway 3 was determined. These partial quantum yields are consistent with the experimental observation and reaction mechanism for the following reasons. First, the formation of DMA result from both pathways 1 and 2, where the pathway 1 has smaller partial quantum yields than pathway 2 by 10 times at pH 7 and 3.6 times at pH 3. The significantly smaller quantum yield of pathway 1 is consistent with the experimental observation.[9] Second, similar partial quantum yields of pathway 2 determined at both pH values in this study (*i.e.*, 0.2 at pH 7 and 0.18 at pH 3) are consistent with the experimental observation of similar amounts of NO_2^- produced at both pH values,[9] although the highest yield was observed at pH 4. The highest yield at pH 4 was proved by the fact that the

Table 1 Photochemical elementary reaction pathways with theoretically calculated aqueous-phase free energies of activation and reactions, and reaction rate constants. All thermodynamic and kinetics parameters were theoretically calculated by this study. The quantum yields, reactions rate constants, and equilibrium constants that were obtained from previous studies in the literature, and otherwise, estimated by this study

Pathway no.	Mechanisms	Elementary reaction	Quantum yield of products	Molar absorptivity, M^{-1} cm^{-1}	Reference for quantum yields
1	Photolysis	$(CH_3)_2N–NO–H^+ \rightarrow (CH_3)_2{}^{\bullet}NH^+ + NO^{\bullet}$	0.02 (pH = 7) and 0.05 (pH = 3)[a]	1650	
2	Photolysis	$(CH_3)_2N–NO–H^+ \rightarrow (CH_3)_2NH_2^+ + HNO_2$	0.20 (pH = 7) and 0.18 (pH = 3)[a]		
3	Photolysis	$(CH_3)_2N–NO–H^+ \rightarrow CH_2{=}N^+HCH_3 + NO^{\bullet} + O_2^{\bullet-}$	0.12 (pH = 7) and 0.27 (pH = 3)[a]		
4	Photolysis	$NO_3^- \rightarrow [NO_3^-]^* \rightarrow NO_2^{\bullet} + O^{\bullet-}$	0.037	15	48
5	Photolysis	$NO_3^- \rightarrow [NO_3^-]^* \rightarrow ONOO^-$	0.102	15	48
6	Photolysis	$NO_2^- \rightarrow [NO_2^-]^* \rightarrow NO^{\bullet} + O^{\bullet-}$	0.02	32	48
7	Photolysis	$ONOO^- \rightarrow [ONOO^-]^* \rightarrow NO^{\bullet} + O_2^{\bullet-}$	0.1	555	49

Pathway no.	Mechanisms	Elementary reaction	$\Delta G^{act}_{aq,calc}$, kcal mol^{-1}	$\Delta G^{react}_{aq,calc}$, kcal mol^{-1}	$\Delta E^{act}_{aq,calc}$, kcal mol^{-1}	Imaginary frequency	k, M^{-1} s^{-1} unless noted	Reference for rate constants
8	Radical coupling	$(CH_3)_2{}^{\bullet}NH^+ + {}^{\bullet}NO \rightarrow CH_3N(+)H{=}CH_2 + HNO$	9.9	−12.0	−3.8	−743.5	7.2×10^8	7, 9
9	Dimerization	$2HNO \rightarrow HN(OH)–N{=}O$	9.5	−33.4	−3.2	−1773.3	8.0×10^6 s^{-1}	50
10	Cleavage of N–O bond	$HN(OH)–N{=}O \rightarrow N_2O + H_2O$	53.3	−60.0	57.0	−1874.9		
11	Hydrolysis	$CH_3N(+)H{=}CH_2 + H_2O \rightarrow CH_3NH_3^+ + HCHO$	34.0	5.2	22.6	−1585.7	1.0×10^3 s^{-1}	[d]
12	1,2-H shift	$(CH_3)_2{}^{\bullet}N \rightarrow {}^{\bullet}CH_2NHCH_3$	31.6 (2 explicit water molecules)	2.6	12.9	−303.6	1.0×10^6 s^{-1}	[d]
13	O_2 addition	${}^{\bullet}CH_2NHCH_3 + O_2 \rightarrow {}^{\bullet}OOCH_2NHCH_3$	−13.3 (−7.0[b] and −6.9[c])	−25.3 (−19.2[b] and −22.0[c])	−24.6 (−18.5[b] and −18.3[c])	−118.3 (−85.2[b])	4.5×10^9	[d]
14	Radical coupling	$NO^{\bullet} + O_2^{\bullet-} \rightarrow ONOO^-$	6.8	−9.2	−2.9	−278.9	4.2×10^9	52
15	Radical coupling	$NO^{\bullet} + HO_2^{\bullet} \rightarrow ONOOH$	5.3 (1 explicit water molecule)	−9.6 (*trans*) −11.6 (*cis*)	−16.4	−194.1	3.2×10^9	52
16	Radical coupling	$NO^{\bullet} + HO^{\bullet} \rightarrow HNO_2$	5.5	−37.1	−0.8	−156.7	1.0×10^{10}	52
17	Radical coupling	$NO_2^{\bullet} + HO^{\bullet} \rightarrow ONOOH$	−13.4	−45.7	−23.4	−674.8	4.5×10^9	53
18	Radical coupling	$NO_2^{\bullet} + O^{\bullet-} \rightarrow ONOO^-$	−4.9	−61.3	−13.1	−760.8	3×10^9	54
19	Radical coupling	$NO^{\bullet} + NO_2^{\bullet} \rightarrow N_2O_3$	8.0	−2.7	−2.7	−165.2	1.1×10^9	55
20	Radical coupling	$NO_2^{\bullet} + NO_2^{\bullet} \rightarrow N_2O_4$	5.0	−5.1	−2.1	−26.9	4.5×10^8	56
21	Radical coupling	$NO^{\bullet} + NO^{\bullet} + (O_2) \rightarrow 2NO_2^{\bullet}$	26.3[c]	−9.2[c]	5.0[c]	−257.7[c]	1.0×10^9	57
22	Isomerization	$ONOO^- \rightarrow NO_3^-$	48.5	−50.9	49.7	−1446	8.0×10^{-6} s^{-1}	54
23	Isomerization	$ONOOH \rightarrow NO_3^- + H^+$	38.9 (2 explicit water molecules)	−88.9	29.3	−506.4	0.65 s^{-1}	58, 59
24	Radical coupling	$HO_2^{\bullet} + NO_2^{\bullet} \rightarrow OONOOH$	−25.5	−46.8	−37.8	−170.3	1.8×10^9	60, 61

Table 1 *(continued)*

Pathway no.	Mechanisms	Elementary reaction	Quantum yield of products	Molar absorptivity, M^{-1} cm^{-1}	Reference for quantum yields			
25	Radical coupling	$O_2^{\bullet-} + NO_2^{\bullet}$ $\rightarrow$ $OONOO^-$	−28.2	−47.8	−38.2	−92.5	4.5×10^9	60, 61
26	Single electron transfer	$NO_2^- + HO^{\bullet}$ $\rightarrow$ $NO_2^{\bullet} + OH^-$	3.5	−2.7	—	—	6.0×10^9	53
27	Adduct formation	$HCHO^{\bullet} + ONOO^-$ $\leftrightarrow$ $H_2C(ONOO^-)O$	8.4 (*trans*) and 11.9 (*cis*) (forward)3.8 (*trans*) and 7.3 (*cis*) (backward)	4.6 (*trans*) and 8.3 (*cis*) (forward)−4.6 (*trans*) and −8.3 (*cis*) (backward)	−3.3	−186.9	—	[d]
28	Hydrolysis	$HCHO + H_2O$ $\rightarrow$ $CH_2(OH)_2$	31.5	−1.2	8.6	−812.8	10 s^{-1} (neutral)5.4 × 10^3 s^{-1} (acidic)	46, 47
29	H abstraction	$CH_2(OH)_2 + HO^{\bullet}$ $\rightarrow$ $^{\bullet}CH(OH)_2 + H_2O$	8.8	−24.9	3.2	−881.4	7.4×10^7	[d]
30	H abstraction	$CH_2(OH)_2 + ONOO^-$ $\rightarrow$ $^{\bullet}CH(OH)_2 + {}^{\bullet}NO_2 + OH^-$	40.1	−11.4	33.3	−1089.7	2.5×10^4	[d]
31	H abstraction	$CH_2(OH)_2 + ONOOH$ $\rightarrow$ $^{\bullet}CH(OH)_2 + {}^{\bullet}NO_2 + H_2O$	53.4	−14.5	46.1	−996.9	1.0×10^4	[d]
32	O_2 addition	$^{\bullet}CH(OH)_2 + O_2 \rightarrow$ $^{\bullet}OOCH(OH)_2$	−9.7 (−8.3[b] and −5.1[c])	−32.9 (−28.3[b] and −30.7[c])	−21.8 (−19.7[b] and −17.2[c])	−231.9 (−77.8[b])	4.8×10^9	[d]
33	Unimolecular decay	$^{\bullet}OOCH(OH)_2 \rightarrow HO_2^{\bullet}$ $+ HCOOH$	9.2	−9.1	11.9	−969.2	8.7×10^3 s^{-1}	23
34	H-Abstraction	$HCOOH + HO^{\bullet} \rightarrow {}^{\bullet}COOH$ $+ H_2O$	10.5	−18.1	4.9	−1103.1	4.5×10^7	23
35	H-Abstraction	$HCOO^- + HO^{\bullet} \rightarrow {}^{\bullet}COO^-$ $+ H_2O$	5.2	−31.0	−1.4	−790.6	2.4×10^9	23
36	Single electron transfer	$^{\bullet}COO^- + O_2 \rightarrow {}^{\bullet}O_2^- + CO_2$	2.3	−33.1	—	—	2.4×10^9	62

	Species	Equilibrium reaction	pK_a	Reference
37	NDMA	$(CH_3)_2NNO\text{–}H^+ \leftrightarrow$ $(CH_3)_2NNO + H^+$	8.5	6
38	Aminium radical	$(CH_3)_2{}^{\bullet}NH^+ \leftrightarrow (CH_3)_2{}^{\bullet}N +$ H^+	6.5	63
39	Dimethylamine	$(CH_3)_2NH_2^+ \leftrightarrow (CH_3)_2NH$ $+ H^+$	10.77	64
40	Methylamine	$CH_3NH_3^+ \leftrightarrow CH_3NH_2^+ +$ H^+	10.64	64
41	Peroxynitrous	$ONOOH \leftrightarrow ONOO^- + H^+$	6.6	65
42	Peroxynitric acid	$O_2NOOH \leftrightarrow O_2NOO^- + H^+$	5.85	52
43	Hydroperoxyl radical	$HO_2^{\bullet} \leftrightarrow O_2^{\bullet-} + H^+$	4.8	66
44	Nitrate	$HNO_3 \leftrightarrow NO_3^- + H^+$	−1.38	64
45	Nitrite	$HNO_2 \leftrightarrow NO_2^- + H^+$	3.2	64
46	Hydroxyl radical	$HO^{\bullet} \leftrightarrow O^{\bullet-} + H^+$	11.9	67
47	Hydrogen peroxide	$H_2O_2 \leftrightarrow HO_2^- + H^+$	11.6	64

[a] Determined in this study, see text. [b] Obtained at the level of UM05/Aug-cc-pVTZ. [c] Obtained at the single point energy with UCCSD(T)/cc-pVTZ for the structure obtained at UM05/Aug-cc-pVTZ. [d] Estimated based on the $\Delta G_{aq,calc}^{act}$ value and previously developed LFERs.[19,21]

formation of HNO_2/NO_2^- result from the acid-catalyzed mechanisms of pathway 2 alone.[7] The sum of the partial quantum yields should be equal to that of the overall pathway if each species in the specific pathway does not participate in the other photochemical reactions.[68] While the sum of the quantum yields at pH 7 was determined to be 0.34 which is consistent with the experimental value, the overall calculated quantum yield of 0.50 at pH 3 was significantly larger than the experimental value (0.31). In particular, the quantum yield of 0.27 determined for pathway 3 at pH 3 is significantly larger than 0.12 at pH 7 for photolysis pathway 3. Two major possibilities could explain this discrepancy: (1) the non-cage reaction of pathway 3 and (2) the way of determining the partial quantum yield. Unlike pathways 1 and 2, pathway 3 does not occur in cage but is catalyzed by dissolved oxygen. Thus, the products of pathway 3 do not necessarily result from the direct photolysis of NDMA. However, the dependency of non-cage reaction on the solution pH is not clear as the dissolved oxygen concentrations at both pH values do not differ significantly and the concentration profiles of NDMA and other products were obtained in O_2-saturated solution experimentally.[9] The other possible reason is that we determined the partial quantum yield based on the available experimentally determined time-dependent concentration decays of NDMA, DMA, MA, nitrate and nitrite but with no experimental information on the concentrations of species involved in pathway 3 (*i.e.*, *N*-methylidenmethylamine, $NO^•$ and $O_2^{•-}$). The experimental data showed a more significant decrease in the nitrate formation yield at pH 7 under N_2-saturated condition (*i.e.*, non-oxygenated solution) than at pH 3.[7] This indicates that the production of $NO^•$ and $O_2^{•-}$ from the pathway 3 is key for the formation of nitrate through reactions 14 and 19. Thus, the nitrate concentration profile dominantly determined the partial quantum yield at pH 7 but did not necessarily determine the quantum yield for the formation of $NO^•$ and $O_2^{•-}$. Because of this reason, we may have obtained significantly larger partial quantum yield (*i.e.*, 0.27). At pH 3, the nitrate formation was not significantly affected by different experimental conditions (*i.e.*, O_2- and N_2-saturated solutions).[7] Our determined partial quantum yield (*i.e.*, 0.12) at pH 3 is consistent with the experimental value of 0.144[9] determined from the formation yield of $O_2^{•-}$ at pH 7, indicating that the formation of $O_2^{•-}$ from pathway 3 is pH-independent. The concentration profile of methylamine is affected by the formation of *N*-methylidenmethylamine that is produced by both pathway 3 and radical reaction of pathway 8. Given that our predicted time-dependent concentration profile of MA is consistent with experimental observations at both pH values (Fig. 1), the partial quantum yield of 0.12 for the formation of *N*-methylidenmethylamine at pH 3 should also represent that at pH 7. It should be noted that we determined the partial quantum yields using the concentration profiles for ~15 minutes but experimental data are also available at pH 7 for up to 300 minutes for higher NDMA initial concentration.[7] While there is an approach to theoretically calculate the quantum yield for the elementary reaction pathways,[69] uncertainty remains and it could be applied for only small molecular size compounds. More mechanistic investigation on each photolysis pathway is needed.

Radical-involved reactions

The aminium radical $[(CH_3)_2{}^•NH^+]$ and the $NO^•$ produced in pathway 1 react in a solvent cage to produce *N*-methylidenmethylamine. The pK_a of aminium radicals is 6.5,[64] and approximately 75% of the total concentration is present in a nonprotonated form at pH 7; the protonated form is dominant at pH 3. The protonated aminium radical reacts with $NO^•$ undergoing a radical–radical coupling at 9.9 kcal mol^{-1} of the $\Delta G^{act}_{aq,calc}$ value and producing methylidenmethylamine and HNO (reaction 8). The HNO produced in reaction 8 undergoes dimerization and arrangement to produce the final product of N_2O and H_2O ($k = (8 \pm 3) \times 10^6\ M^{-1}\ s^{-1}$).[50] The overall reaction contains two elementary reaction steps: (1) the formation of HN(OH)–N=O *via* dimerization of HNO at the $\Delta G^{act}_{aq,calc}$ value of 9.5 kcal mol^{-1} (reaction 9) and (2) arrangement by cleaving the N–O bond of HN(OH) to produce N_2O and H_2O at the $\Delta G^{act}_{aq,calc}$ value of 53.3 kcal mol^{-1} (reaction 10). Methylidenmethylamine undergoes hydrolysis to produce MA and HCHO (reaction 11) and the first order rate constant, $10^3\ s^{-1}$, is used based on the similar hydrolysis reaction with previously determined $\Delta G^{act}_{aq,calc}$ value.[46,47] Nonprotonated aminium radicals have an unpaired electron adjacent to an electron lone pair, and conjugative delocalization transfers the unpaired electron of the N-centered radical to the carbon,[70,71] which produces a carbon-centered radical, $^•CH_2NHCH_3$ (reaction 12). Unlike the addition of molecular oxygen to a carbon-centered radical, this delocalization of the radical spin density causes an N-centered radical to undergo abnormally slow reactions for molecular oxygen addition (*i.e.*, $5.3 \times 10^6\ M^{-1}\ s^{-1}$)[71] and results in no competition with the unimolecular H-shift from an alkoxyl radical to a C-centered radical ($\sim 1.0 \times 10^6\ s^{-1}$).[51] Since no experimentally measured first-order reaction rate has been reported for this H-shift reaction, we used $1.0 \times 10^6\ s^{-1}$, as estimated based on the similar H-shift from the C-centered radical and the similar $\Delta G^{act}_{aq,calc}$ value.[51] Our calculations obtained 31.6 kcal mol^{-1} of $\Delta G^{act}_{aq,calc}$ for the H-shift of the N-centered radical with two-explicit water molecules and the $\Delta G^{react}_{aq,calc}$ value indicates the slight endergonic reaction. Text S8 in the ESI† includes the detailed procedure to calculate the thermodynamic parameters in the presence of explicit water molecules. The carbon-centered radical further reacts with dissolved oxygen to produce the peroxyl radical ($CH_3NHCH_2OO^•$) (reaction 13). The $\Delta G^{act}_{aq,calc}$ value is −13.3 kcal mol^{-1}, which was used to estimate the rate constant using the previously developed LFER.[19] We have investigated the impact of multireference state and spin flip of this addition reaction in Text S2 in the SI. The peroxyl radicals undergo uni-/bimolecular decay to produce various intermediates, including CH_3NHCHO, $CH_3NHCH_2O^•$, CH_3NHCH_2OH, and $CH_3N^+H{=}CH_2$ *via* the Bennett reaction mechanism[72,73] and other bimolecular reactions that produce the alkoxyl radical[74] and the alcohol *via* the Russell mechanism.[75] Lee *et al.* reported the production of CH_3NHCHO from NDMA photolysis at approximately neutral pH values (pH 5.5–8) in a deoxygenated environment and proposed the reaction of $^•NO$ with $^•CH_2NHCH_3$.[7] This finding indirectly supports the pathway of peroxyl radical bimolecular decay for the formation of CH_3NHCHO in an oxygenated environment. The other reaction pathway induced by $NO^•$ will be discussed for pathway 3.

DMA and nitrous acid (HNO_2) are produced by the homolytic pathway 2 of NDMA photolysis. DMA, whose pK_a is 10.77, is present as protonated DMA [*i.e.*, $(CH_3)_2NH_2^+$] at both pH 7 and pH 3. There is no other pathway to produce DMA in NDMA degradation, and thus, DMA formation was solely used to determine the partial quantum yield of pathway 2 (*i.e.*, 0.20 at pH 7 and 0.18 at pH 3). HNO_2, whose pK_a is 3.2, is present as nitrite as the dominant form at pH 7, but both HNO_2 and nitrite are present at pH 3. The photochemical fate of nitrite is discussed in the section below. Although the nitrogen of DMA reacts with $HO^•$ *via* single electron transfer to produce a two-electron three-centered (2e–3c) adduct, and H-atom abstraction from a C–H bond of methyl functional groups occurs to produce a carbon-centered radical,[76] the apparent low concentration of $HO^•$ in UV photolysis ($10^{-13–-14}$ M at pH 7 and $10^{-13–-12}$ M at pH 3) makes this reaction insignificant. Consequently, the formation of DMA was dominant and became saturated as NDMA decay slowed at the later reaction time (Fig. 1).

N-Methylidenmethylamine, $NO^•$ and $O_2^{•-}$ are produced by photooxidation pathway 3 of NDMA photolysis. $NO^•$ reacts with $HO_2^•/O_2^{•-}$ (pK_a = 4.8)[67] in the solvent cage to produce $ONOOH/ONOO^-$ (pK_a = 6.6)[66] in reactions 14 and 15 (Table 1). The $\Delta G^{act}_{aq,calc}$ values for the reaction with $O_2^{•-}$ is 6.8 kcal mol^{-1} and this is an exergonic reaction at the $\Delta G^{react}_{aq,calc}$ value of −9.2 kcal mol^{-1}. We obtained 5.3 kcal mol^{-1} of $\Delta G^{react}_{aq,calc}$ value in the presence of one explicit water as the water molecule stabilizes the reactants in reaction 15 and confirmed the products of ONOOH at −9.6 kcal mol^{-1} for the *trans* and −11.6 kcal mol^{-1} for the *cis* form, respectively. $NO^•$ also reacts with $HO^•$ to produce HNO_2 with 5.5 kcal mol^{-1} of the $\Delta G^{act}_{aq,calc}$ value (reaction 16). ONOOH and dissociated form, $ONOO^-$, are also produced by the reaction of $HO^•/O^{•-}$ with $NO_2^•$ (reactions 17 and 18),[54,55] which is the product of nitrate photolysis. The negative $\Delta G^{act}_{aq,calc}$ values of reactions 17 and 18 (and reactions 26 and 27) imply the possible formation of precursor-complexes; however, we were not able to optimize the loosely bound structures of any precur-complexes. The single Slater determinant formalism used in DFT may have caused issues in calculating the potential energy surface for interactions of two multicenter free radicals, although the gaseous phase NO_2–NO_2 isomers were determined with several post *ab initio* and DFT methods including a mutireference method.[26] The use of a multireference method for aqueous-phase reactions is beyond the scope of this study but we are now investigating the cause of possible errors. Because of the uncertainties of these negative values, we did not include these datapoints in the analysis of a linear free energy relationship shown below. $NO^•$ reacts with $NO_2^•$ to produce a short-lived intermediate, N_2O_3 (reaction 19) at the $\Delta G^{act}_{aq,calc}$ value of 8.0 kcal mol^{-1}. Similar reactions occur for the disproportionation reaction of $NO_2^•$ (reaction 20), which produces N_2O_4 and the ultimate products of NO_2^- and NO_3^-.[50] Our theoretical calculation indicates that the disproportionation of $NO_2^•$ requires 5.0 kcal mol^{-1} of $\Delta G^{act}_{aq,calc}$. While our transition state clearly showed the nitrogen–nitrogen radical coupling and confirmed by the IRC analysis, small imaginary frequency and unexpectedly small free energy of activation for the reported rate constant ($k = 4.5 \times 10^8$ M^{-1} s^{-1}) raises concern about our value. We were not able to locate the transition state with other methods and no studies in both gaseous and aqueous phases reported the transition state structures. The disproportionation of $NO^•$ in the presence of molecular oxygen (reaction 21) requires 26.3 kcal mol^{-1} of $\Delta G^{act}_{aq,calc}$. $ONOO^-$ or ONOOH undergoes an isomerization reaction to produce NO_3^-. Our calculation indicates 48.5 kcal mol^{-1} or 38.9 kcal mol^{-1} of $\Delta G^{act}_{aq,calc}$ (reactions 22 and 23). While $ONOO^-$ is very stable, as verified by the experimental k value of 8.0×10^{-6} s^{-1},[54] ONOOH undergoes much faster decay (*i.e.*, k = 0.65 s^{-1}).[59,60] The *cis*-form of ONOOH undergoes O–O bond cleavage as a result of orbital interactions between the two separating parts of the ONO⋯HO radical pair to produce an activated species, $HOONO^•$.[59,60] This activated species eventually produces HNO_3.

$NO_2^•$ reacts with $O_2^{•-}/HO_2^•$ to produce peroxynitric acid/peroxynitrate ($OONOOH/OONOO^-$), which are stronger acids than $ONOOH/ONOO^-$.[48] The pK_a of peroxynitric acid is 5.8,[52] and OONOOH is dominant at weakly acidic and neutral pH values. The formation of OONOOH and $OONOO^-$ requires −25.5 kcal mol^{-1} and −28.2 kcal mol^{-1} of $\Delta G^{act}_{aq,calc}$ (reactions 24 and 25).

Pathway from HCHO to HCOOH

At 254 nm, HCHO does not have a noticeable absorbance (Fig. S4 of the ESI†). Thus, the direct photolysis pathway from HCHO to HCOOH is not feasible. HCHO and the hydrolyzed form of $CH_2(OH)_2$ may undergo $HO^•$ reactions and produce HCOOH as the ultimate product.[23] Merényi *et al.* calculated a yield of 30–40% for $HO^•$ + $NO_2^•$ from the HCOOH decay.[77] However, the experiment was performed with a pulse radiolysis system and utilized a high concentration of nitrite (*i.e.*, 0.06–6.5 mM NO_2^-) to generate ONOOH. In the NDMA photolysis, $HO^•$ that is produced by multiple radical pathways reaches considerably lower concentrations, such that, in our kinetic model $HO^{\bullet}$ does not contribute significantly to the formation of HCOOH from $HCHO/CH_2(OH)_2$. One possible reaction pathway is the oxidation of HCHO or $CH_2(OH)_2$ by $ONOO^-/ONOOH$. The $ONOO^-/ONOOH$ abstracts a H-atom from a C–H bond of $CH_2(OH)_2$ to produce carbon-centered radicals.[9] The $\Delta G^{act}_{aq,calc}$ values for these reactions are 40–54 kcal mol^{-1} (reactions 30 and 31). Due to the unavailable kinetic data about these reactions, we estimated the *k* values (2.5×10^4 M^{-1} s^{-1} for reaction 30 and 1.0×10^4 M^{-1} s^{-1} for reaction 31) for both reactions based on our $\Delta G^{act}_{aq,calc}$ values and the previously developed LFER[21] for H-atom abstraction by $HO^{\bullet}$. The orders of estimated rate constants are consistent with the experimental *k* value observed for similar compounds with $ONOO^-/ONOOH$.[78] It should be noted that previous LFER was develop based on the G1–G4 methods[21] and our $\Delta G^{act}_{aq,calc}$ values were calculated with M06-2X/Aug-cc-pVTZ and thus a few energy differences resulting from two different methods are present. The concentrations of $ONOO^-/ONOOH$ are approximately 10^{-8} M and are significantly higher than those of other radical species. Thus, even though smaller rate constant of about 10^4 M^{-1} s^{-1}, the reaction products (*i.e.*, carbon centered radicals and subsequent HCOOH) are significant (see the discussion below).

$ONOO^-$ also attacks the carbonyl group of HCHO nucleophilically (reaction 27), producing an intermediate, $H_2C(ONOO^-)O$, in cages.[78,79] The intermediate undergoes three possible reactions: (1) in-cage isomerization to produce HCHO and NO_3^-; (2) electron transfer to produce $HCOO^-$, NO_2^-, and H^+; and (3) cleavage of the O–N bond to produce $NO_2^{\bullet}$ and alkoxyl radicals.[79,80] However, this reaction is an endergonic reaction, indicating a faster backward reaction. Thus, we believe the reaction 27 does not significantly contribute to the formation of products that are involved in the subsequent reactions. The calculated relative probability is that at the point of 10 minutes reaction time, 78% and 22% of $ONOO^-$ reacts with $CH_2(OH)_2$ and HCHO, respectively, at pH 7. At pH 3 for the same reaction time, 91% and 19% of $ONOO^-$ reacts with $CH_2(OH)_2$ and HCHO, respectively. $HCOO^-/HCOOH$ is the end product of NDMA oxidation and is mineralized into CO_2 (reactions 34–36). Fig. S5 of the ESI† summarizes all the reaction pathways of the NDMA initial transformation induced by photolysis.

Photochemical fate of reactive nitrogen species

Reactive nitrogen species are the initial intermediate products of the photolysis of nitrate, nitrite and $ONOO^-/ONOOH$, and therefore, these photochemical reactions are included in our kinetic model. Photolysis of nitrate at 254 nm (15 M^{-1} cm^{-1} of molar absorptivity, ε, at 254 nm) follows two pathways: (1) the production of $NO_2^{\bullet}$ and $O^{\bullet-}$ with 0.037 quantum yield and (2) the production of $ONOO^-$ with a quantum yield of 0.102.[48] $O^{\bullet-}$ is the conjugate base of $HO^{\bullet}$ ($pK_a = 11.9$),[68] and the photolysis of nitrate is the major source of $HO^{\bullet}$. The photolysis of nitrite ($\varepsilon = 32$ M^{-1} cm^{-1}) produces $NO^{\bullet}$ and $O^{\bullet-}$ with a quantum yield of 0.02.[48] Nitrite also reacts with $HO^{\bullet}$ *via* single electron transfer to form $NO_2^{\bullet}$. The calculated $\Delta G^{act}_{aq,calc}$ using the Marcus theory[41,42] (see Text S3 in the ESI† for a detailed procedure) is 3.5 kcal mol^{-1} (reaction 26). Finally, $ONOO^-$ has a significantly larger molar absorptivity (*i.e.*, $\varepsilon = 555$ M^{-1} cm^{-1}) than those of nitrate and nitrite, and the photolysis reaction produced $NO^{\bullet}$ and $O_2^{\bullet-}$ with a quantum yield of 0.1.[49] All photochemical pathways of nitrate, nitrite, and $ONOO^-/ONOOH$ identified in this study and compiled based on past experimental studies are summarized in Fig. S6 of the ESI.† The eventual products of these photochemical pathways are nitrate and nitrite.

Linear free energy relationship for reactive nitrogen species

Although the number of datasets is small ($N = 5$), we have developed a linear free energy relationship between the $\Delta G^{act}_{aq,calc}$ values and ln*k*. The detailed development and evaluation is provided in Text S9 and Fig. S7 of the ESI.†

Conclusions

This study highlights the elementary reaction pathways and kinetics of reactive nitrogen species and oxygenated radicals that are produced in the photolysis of NDMA in the aqueous phase. In particular, the photochemical reactions of nitrogen-centered radicals, peroxynitrous acid/peroxynitrite, and peroxynitric acid/peroxynitrite are studied, and the aqueous-phase free energies of activation and reaction are determined to advance our understanding of the fate of nitrosamine compounds in the water treatment process. The photochemical reactions of these reactive nitrogen species in oxygenated environments occur in natural aquatic systems for nitrogen-containing anthropogenic compounds (*e.g.*, pesticides and herbicides) and atmospheric water droplets in clouds for nitrate, nitrite, and nitric oxide. Similar reactions also occur in human cells, where the toxic substances peroxynitrous acid/peroxynitrite play important roles because of the potential damage to cells, which may cause the formation of cancer cells. Our study also provides mechanistic insight into reaction mechanisms in emerging AOPs that utilize the combination of UV with chloramine in water reclamation processes. Given that many toxic chemicals contain nitrogen species, it is important to develop a fundamental kinetic model that can be used to predict the fate of nitrogen-containing species in various environmental processes. Finally, the elementary reaction-based kinetic model developed in this study contains general water quality and photolysis operational parameters. Thus, the validated model can be used to simulate the photochemical decay of nitrosamines in real water with possible addition of other water quality parameters such as alkalinity, co-presented ions, and dissolved organic matter.

Conflicts of interest

There are no conflicts to declare.

Acknowledgements

This work was partially supported by the National Science Foundation Award: CHE-1808052. Any opinions, findings, conclusions, or recommendations expressed in this publication are those of the authors and do not necessarily reflect the view of the supporting organization. E.C. appreciates the scholarship from AWWA through the 2018 Carollo/Bryant L. Bench Scholarship and Michigan Space Grant Consortium fellowship. Finally, the authors appreciate the support from the Michigan Tech HPC cluster 'Superior'.

Notes and references

1 US EPA, Six-year review 3 technical support document for nitrosamines. Office of Water (4607M), EPA 810-R-16-009. 2016, (accessed April 2021).

2 Y. Qian, M. Wu, W. Wang, B. Chen, H. Zheng, S. W. Krasner, S. E. Hrudey and X.-F. Li, Determination of 14 Nitrosamines at Nanogram per Liter Levels in Drinking Water, *Anal. Chem.*, 2015, **87**, 1330–1336.

3 W. A. Mitch, J. O. Sharp, R. R. Trussell, R. L. Valentine, L. Alvarez-Cohen and D. L. Sedlak, N-Nitrosodimethylamine (NDMA) as a Drinking Water Contaminant: A Review, *Environ. Eng. Sci.*, 2003, **20**, 389–404.

4 US EPA, Technical fact sheet- N-Nitroso-dimethylamine (NDMA). November 2017, https://www.epa.gov/sites/production/files/2014-03/documents/ffrrofactsheet_contaminant_ndma_january2014_final.pdf, (accessed April 2021).

5 California Water Boards, State Water Resources Control Boards., https://www.waterboards.ca.gov/drinking_water/certlic/drinkingwater/NDMA.html, (accessed April 2020).

6 B. G. Kwon, J.-O. Kim and J.-K. Kwon, Formation of reactive species enhanced by H_2O_2 addition in the photodecomposition of N-nitrosodimethylamine (NDMA), *Environ. Eng. Res.*, 2013, **18**(1), 29–35.

7 C. Lee, W. Choi, Y. G. Kim and J. Yoon, UV Photolytic Mechanism of N-Nitrosodimethylamine in Water: Dual Pathways to Methylamine versus Dimethylamine, *Environ. Sci. Technol.*, 2005, **39**, 2101–2106.

8 M. I. Stefan and J. R. Bolton, UV Direct Photolysis of N-Nitrosodimethylamine (NDMA): Kinetic and Product Study, *Helv. Chim. Acta*, 2002, **85**, 1416–1426.

9 C. Lee, W. Choi and J. Yoon, UV Photolytic Mechanism of N-Nitrosodimethylamine in Water: Roles of Dissolved Oxygen and Solution pH, *Environ. Sci. Technol.*, 2005, **39**, 9702–9709.

10 D. Tsikas, GC-MS and HPLC methods for peroxynitrite (ONOO− and O15NOO−) analysis: a study on stability, decomposition to nitrite and nitrate, laboratory synthesis, and formation of peroxynitrite from S-nitrosoglutathione (GSNO) and KO2, *Analyst*, 2011, **136**, 979–987.

11 J. Mack and J. R. Bolton, Photochemistry of nitrite and nitrate in aqueous solution: a review, *J. Photochem. Photobiol., A*, 1999, **128**, 1–13.

12 S. Goldstein and J. Rabani, Mechanism of Nitrite Formation by Nitrate Photolysis in Aqueous Solutions: The Role of Peroxynitrite, Nitrogen Dioxide, and Hydroxyl Radical, *J. Am. Chem. Soc.*, 2007, **129**, 10597–10601.

13 G. Mark, H.-G. Korth, H.-P. Schuchmann and C. von Sonntag, The photochemistry of aqueous nitrate ion revisited, *J. Photochem. Photobiol., A*, 1996, **101**, 89–103.

14 H. O. N. Tugaoen, S. Garcia-Segura, K. Hristovski and P. Westerhoff, Challenges in photocatalytic reduction of nitrate as a water treatment technology, *Sci. Total Environ.*, 2017, **599-600**, 1524–1551.

15 D. Trogolo, B. K. Mishra, M. B. Heeb, U. von Gunten and J. S. Arey, Molecular Mechanism of NDMA Formation from N,N-Dimethylsulfamide During Ozonation: Quantum Chemical Insights into a Bromide-Catalyzed Pathway, *Environ. Sci. Technol.*, 2015, **49**, 4163–4175.

16 R. Xiao, M. Noerpel, H. Ling Luk, Z. Wei and R. Spinney, Thermodynamic and kinetic study of ibuprofen with hydroxyl radical: A density functional theory approach, *Int. J. Quantum Chem.*, 2014, **114**, 74–83.

17 T. An, Y. Gao, G. Li, P. V. Kamat, J. Peller and M. V. Joyce, Kinetics and Mechanism of •OH Mediated Degradation of Dimethyl Phthalate in Aqueous Solution: Experimental and Theoretical Studies, *Environ. Sci. Technol.*, 2014, **48**, 641–648.

18 D. Minakata, W. Song, S. P. Mezyk and W. J. Cooper, Experimental and theoretical studies on aqueous-phase reactivity of hydroxyl radicals with multiple carboxylated and hydroxylated benzene compounds, *Phys. Chem. Chem. Phys.*, 2015, **17**, 11796–11812.

19 D. Minakata, S. P. Mezyk, J. W. Jones, B. R. Daws and J. C. Crittenden, Development of Linear Free Energy Relationships for Aqueous Phase Radical-Involved Chemical Reactions, *Environ. Sci. Technol.*, 2014, **48**, 13925–13932.

20 D. Minakata, W. Song and J. Crittenden, Reactivity of Aqueous Phase Hydroxyl Radical with Halogenated Carboxylate Anions: Experimental and Theoretical Studies, *Environ. Sci. Technol.*, 2011, **45**, 6057–6065.

21 D. Minakata and J. Crittenden, Linear Free Energy Relationships between Aqueous phase Hydroxyl Radical Reaction Rate Constants and Free Energy of Activation, *Environ. Sci. Technol.*, 2011, **45**, 3479–3486.

22 D. Minakata, D. Kamath and S. Maetzold, Mechanistic Insight into the Reactivity of Chlorine-Derived Radicals in the Aqueous-Phase UV–Chlorine Advanced Oxidation Process: Quantum Mechanical Calculations, *Environ. Sci. Technol.*, 2017, **51**, 6918–6926.

23 D. Kamath, S. P. Mezyk and D. Minakata, Elucidating the Elementary Reaction Pathways and Kinetics of Hydroxyl Radical-Induced Acetone Degradation in Aqueous Phase Advanced Oxidation Processes, *Environ. Sci. Technol.*, 2018, **52**, 7763–7774.

24 D. Kamath and D. Minakata, Emerging investigators series: ultraviolet and free chlorine aqueous-phase advanced

oxidation process: kinetic simulations and experimental validation, *Environ. Sci.: Water Res. Technol.*, 2018, **4**, 1231–1238.

25 S. Naumov and C. von Sonntag, Standard Gibbs Free Energies of Reactions of Ozone with Free Radicals in Aqueous Solution: Quantum-Chemical Calculations, *Environ. Sci. Technol.*, 2011, **45**, 9195–9204.

26 W.-G. Liu and W. A. Goddard, First-Principles Study of the Role of Interconversion Between NO2, N2O4, cis-ONO-NO2, and trans-ONO-NO2 in Chemical Processes, *J. Am. Chem. Soc.*, 2012, **134**, 12970–12978.

27 Y. Zhao, K. N. Houk and L. P. Olson, Mechanisms of Peroxynitrous Acid and Methyl Peroxynitrite, ROONO (R = H, Me), Rearrangements: A Conformation-Dependent Homolytic Dissociation, *J. Phys. Chem. A*, 2004, **108**, 5864–5871.

28 O. B. Gadzhiev, S. K. Ignatov, A. G. Razuvaev and A. E. Masunov, Quantum Chemical Study of Trimolecular Reaction Mechanism between Nitric Oxide and Oxygen in the Gas Phase, *J. Phys. Chem. A*, 2009, **113**, 9092–9101.

29 M. J. Frisch, *GAUSSIAN 16 (Revision D.01)*, Gaussian Inc., Wallingford CT, 2016.

30 R. J. Bartlett and G. D. Purvis, Many-body perturbation theory, coupled-pair many-electron theory, and the importance of quadruple excitations for the correlation problem, *Int. J. Quantum Chem.*, 1978, **14**, 561–581.

31 H.-J. Werner, P. J. Knowles, G. Knizia, F. R. Manby, M. Schütz, and others, MOLPRO, version 2019.2, a package of ab initio programs, see https://www.molpro.net.

32 Y. Zhao and D. G. Truhlar, The M06 suite of density functionals for main group thermochemistry, thermochemical kinetics, noncovalent interactions, excited states, and transition elements: two new functionals and systematic testing of four M06-class functionals and 12 other functionals, *Theor. Chem. Acc.*, 2008, **120**, 215–241.

33 P. R. Tentscher, M. Bourgin and U. von Gunten, Ozonation of Para-Substituted Phenolic Compounds Yields p-Benzoquinones, Other Cyclic α,β-Unsaturated Ketones, and Substituted Catechols, *Environ. Sci. Technol.*, 2018, **52**, 4763–4773.

34 A. Galano and J. R. Alvarez-Idaboy, Kinetics of radical-molecule reactions in aqueous solution: A benchmark study of the performance of density functional methods, *J. Comput. Chem.*, 2014, **35**, 2019–2026.

35 Y. Zhao and D. G. Truhlar, Density Functionals with Broad Applicability in Chemistry, *Acc. Chem. Res.*, 2008, **41**, 157–167.

36 A. V. Marenich, C. J. Cramer and D. G. Truhlar, Universal Solvation Model Based on Solute Electron Density and on a Continuum Model of the Solvent Defined by the Bulk Dielectric Constant and Atomic Surface Tensions, *J. Phys. Chem. B*, 2009, **113**, 6378–6396.

37 J. Gräfenstein, E. Kraka, M. Filatov and D. Cremer, Can Unrestricted Density-Functional Theory Describe Open Shell Singlet Biradicals?, *Int. J. Mol. Sci.*, 2002, **3**, 360–394.

38 T. Saito, S. Nishihara, Y. Kataoka, Y. Nakanishi, T. Matsui, Y. Kitagawa, T. Kawakami, M. Okumura and K. Yamaguchi, Transition state optimization based on approximate spin-projection (AP) method, *Chem. Phys. Lett.*, 2009, **483**, 168–171.

39 K. Fukui, The path of chemical reactions - the IRC approach, *Acc. Chem. Res.*, 1981, **14**, 363–368.

40 H. P. Hratchian and H. B. Schlegel, in *Theory and Applications of Computational Chemistry*, ed. C. E. Dykstra, G. Frenking, K. S. Kim and G. E. Scuseria, Elsevier, Amsterdam, 2005, pp. 195–249, DOI: 10.1016/B978-044451719-7/50053-6.

41 R. A. Marcus, Chemical and Electrochemical Electron-Transfer Theory, *Annu. Rev. Phys. Chem.*, 1964, **15**, 155–196.

42 R. A. Marcus, Electron transfer reactions in chemistry. Theory and experiment, *Rev. Mod. Phys.*, 1993, **65**, 599–610.

43 A. C. Hindmarsh and C. W. Gear, *Ordinary differential equation system solver*, UCID-30001 Rev. 3, Lawrence Livermore Laboratory, Livermore, CA., 1974.

44 J. C. Crittenden, S. Hu, D. W. Hand and S. A. Green, A kinetic model for H2O2/UV process in a completely mixed batch reactor, *Water Res.*, 1999, **33**, 2315–2328.

45 M. Rivlin, U. Eliav and G. Navon, NMR Studies of the Equilibria and Reaction Rates in Aqueous Solutions of Formaldehyde, *J. Phys. Chem. B*, 2015, **119**, 4479–4487.

46 J. P. Guthrie, Hydration of Carbonyl Compounds, an Analysis in Terms of Multidimensional Marcus Theory, *J. Am. Chem. Soc.*, 2000, **122**, 5529–5538.

47 P. Greenzaid, Z. Luz and D. Samuel, N.m.r. study of reversible hydration of aliphatic aldehydes and ketones. Part 3.—Isotopic oxygen exchange of acetone, *Trans. Faraday Soc.*, 1968, **64**, 2780–2786.

48 S. Goldstein, J. Lind and G. Merenyi, Reaction of Organic Peroxyl Radicals with •NO2 and •NO in Aqueous Solution: Intermediacy of Organic Peroxynitrate and Peroxynitrite Species, *J. Phys. Chem. A*, 2004, **108**, 1719–1725.

49 V. Shafirovich and S. V. Lymar, Nitroxyl and its anion in aqueous solutions: Spin states, protic equilibria, and reactivities toward oxygen and nitric oxide, *Proc. Natl. Acad. Sci. U. S. A.*, 2002, **99**, 7340–7345.

50 K. G. Konya, T. Paul, S. Lin, J. Lusztyk and K. U. Ingold, Laser Flash Photolysis Studies on the First Superoxide Thermal Source. First Direct Measurements of the Rates of Solvent-Assisted 1,2-Hydrogen Atom Shifts and a Proposed New Mechanism for This Unusual Rearrangement1, *J. Am. Chem. Soc.*, 2000, **122**, 7518–7527.

51 S. Goldstein and G. Czapski, Reactivity of Peroxynitrite versus Simultaneous Generation of •NO and O2•- toward NADH, *Chem. Res. Toxicol.*, 2000, **13**, 736–741.

52 S. Goldstein and G. Czapski, Kinetics of Nitric Oxide Autoxidation in Aqueous Solution in the Absence and Presence of Various Reductants. The Nature of the Oxidizing Intermediates, *J. Am. Chem. Soc.*, 1995, **117**, 12078–12084.

53 G. Merényi, J. Lind, S. Goldstein and G. Czapski, Mechanism and Thermochemistry of Peroxynitrite Decomposition in Water, *J. Phys. Chem. A*, 1999, **103**, 5685–5691.

54 S. Goldstein, J. Lind and G. Merényi, Chemistry of Peroxynitrites as Compared to Peroxynitrates, *Chem. Rev.*, 2005, **105**, 2457–2470.

55 M. Gratzel, S. Taniguchi and A. Henglein, Study with pulse radiolysis of NO-oxidation and equilibrium N_2O_3 = NO+NO_2 in a water solution, *Ber. Bunsenges. Phys. Chem.*, 1970, **74**, 488–492.

56 M. Grätzel, A. Henglein, J. Lilie and G. Beck, Pulsradiolytische Untersuchung einiger Elementarprozesse der Oxydation und Reduktion des Nitritions, *Ber. Bunsenges. Phys. Chem.*, 1969, **73**, 646–653.

57 M. L. McKee, Ab Initio Study of the N2O4 Potential Energy Surface. Computational Evidence for a New N2O4 Isomer, *J. Am. Chem. Soc.*, 1995, **117**, 1629–1637.

58 O. V. Gerasimov and S. V. Lymar, The Yield of Hydroxyl Radical from the Decomposition of Peroxynitrous Acid, *Inorg. Chem.*, 1999, **38**, 4317–4321.

59 G. R. Hodges and K. U. Ingold, Cage-Escape of Geminate Radical Pairs Can Produce Peroxynitrate from Peroxynitrite under a Wide Variety of Experimental Conditions1, *J. Am. Chem. Soc.*, 1999, **121**, 10695–10701.

60 T. Loegager and K. Sehested, Formation and decay of peroxynitrous acid: a pulse radiolysis study, *J. Phys. Chem.*, 1993, **97**, 6664–6669.

61 S. Goldstein, A. Saha, S. V. Lymar and G. Czapski, Oxidation of Peroxynitrite by Inorganic Radicals: A Pulse Radiolysis Study, *J. Am. Chem. Soc.*, 1998, **120**, 5549–5554.

62 G. E. Adams and R. L. Willson, Pulse radiolysis studies on the oxidation of organic radicals in aqueous solution, *Trans. Faraday Soc.*, 1969, **65**, 2981–2987.

63 Y.-L. Chow, Photolysis of N-nitrosoamines, *Tetrahedron Lett.*, 1964, **5**, 2333–2338.

64 D. W. Green and M. Z. Southard, *Perry's Chemical Engineer's Handbook*, 9th edn, McGraw-Hill Education, 2018.

65 L. R. Mahoney, Evidence for the formation of hydroxyl radicals in the isomerization of pernitrous acid to nitric acid in aqueous solution, *J. Am. Chem. Soc.*, 1970, **92**, 5262–5263.

66 B. H. J. Bielski, D. E. Cabelli, R. L. Arudi and A. B. Ross, Reactivity of HO2/O−2 Radicals in Aqueous Solution, *J. Phys. Chem. Ref. Data*, 1985, **14**, 1041–1100.

67 L. M. Dorfman and G. E. Adams, *Reactivity of the hydroxyl radical in aqueous solutions, Reactivity of the hydroxyl radical in aqueous solutions*, U.S. Department of Commerce, National Bureau of Standards, 1973.

68 M. I. Stefan and J. R. Bolton, UV Direct Photolysis of N-Nitrosodimethylamine (NDMA): Kinetic and Product Study, *Helv. Chim. Acta*, 2002, **85**, 1416–1426.

69 H. Herrmann, On the photolysis of simple anions and neutral molecules as sources of O−/OH, SOx− and Cl in aqueous solution, *Phys. Chem. Chem. Phys.*, 2007, **9**, 3935–3964.

70 D. Griller and F. P. Lossing, Thermochemistry of .alpha.-aminoalkyl radicals, *J. Am. Chem. Soc.*, 1981, **103**, 1586–1587.

71 S. P. Mezyk, W. J. Cooper, K. P. Madden and D. M. Bartels, Free Radical Destruction of N-Nitrosodimethylamine in Water, *Environ. Sci. Technol.*, 2004, **38**, 3161–3167.

72 J. E. Bennett and R. Summers, Product Studies of the Mutual Termination Reactions of sec-Alkylperoxy Radicals: Evidence for Non-Cyclic Termination, *Can. J. Chem.*, 1974, **52**, 1377–1379.

73 J. E. Bennett, G. Brunton, J. R. L. Smith, T. M. F. Salmon and D. J. Waddington, Reactions of alkylperoxyl radicals in solution. Part 2.—A kinetic and product study of self-reactions of 2-propylperoxyl radicals between 253 and 323 K, *J. Chem. Soc., Faraday Trans. 1*, 1987, **83**, 2433–2447.

74 C. von Sonntag and H.-P. Schuchmann, The Elucidation of Peroxyl Radical Reactions in Aqueous Solution with the Help of Radiation-Chemical Methods, *Angew. Chem., Int. Ed. Engl.*, 1991, **30**, 1229–1253.

75 G. A. Russell, Deuterium-isotope Effects in the Autoxidation of Aralkyl Hydrocarbons. Mechanism of the Interaction of PEroxy Radicals1, *J. Am. Chem. Soc.*, 1957, **79**, 3871–3877.

76 S. Das and C. v. Sonntag, The Oxidation of Trimethylamine by OH Radicals in Aqueous Solution, as Studied by Pulse Radiolysis, ESR, and Product Analysis. The Reactions of the Alkylamine Radical Cation, the Aminoalkyl Radical, and the Protonated Aminoalkyl Radical, *Z. Naturforsch. B*, 1986, **41**, 505–513.

77 G. Merényi, J. Lind, S. Goldstein and G. Czapski, Mechanism and Thermochemistry of Peroxynitrite Decomposition in Water, *J. Phys. Chem. A*, 1999, **103**, 5685–5691.

78 M. D. Bartberger, L. P. Olson and K. N. Houk, Mechanisms of Peroxynitrite Oxidations and Rearrangements: The Theoretical Perspective, *Chem. Res. Toxicol.*, 1998, **11**, 710–711.

79 L. S. Nakao, D. Ouchi and O. Augusto, Oxidation of Acetaldehyde by Peroxynitrite and Hydrogen Peroxide/Iron(II) Production of Acetate, Formate, and Methyl Radicals, *Chem. Res. Toxicol.*, 1999, **12**, 1010–1018.